Material: Martensitic: F82H
Property: Concentration weight vs. Distance from surface
Condition: tests under oxygen-saturated liquid lead
Data: Experimental

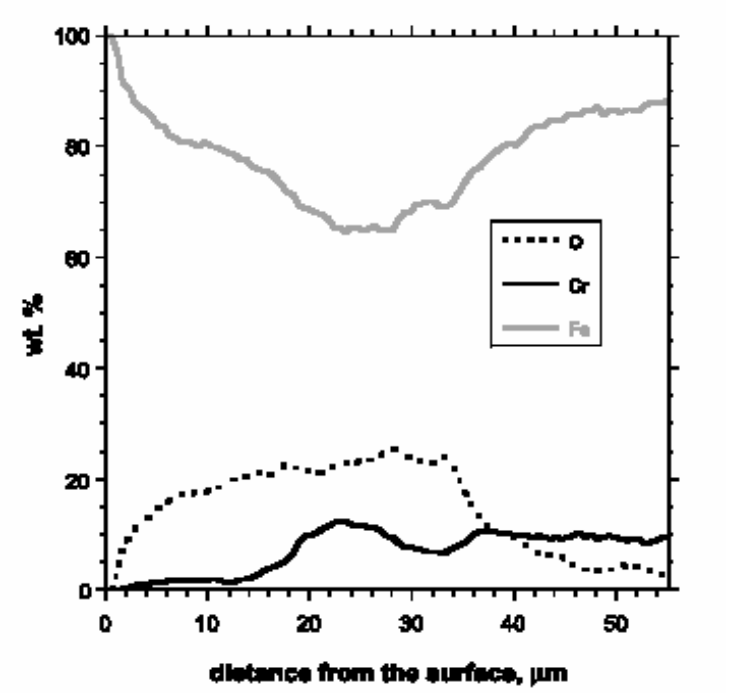

Fig. 3. Concentration line profiles (wt%, EDS analysis with ZAF correction) on a corrosion layer grown on uncoated F82H steel after 3700 h in molten lead at 793 K.

Source:
Journal of Nuclear Materials, 2000, Volume 279, Page 308-316

Title of paper (or report) this figure appeared in:
Behaviour of materials for accelerator driven systems in stagnant molten lead

Author of paper or graph:
Gianluca Benamati, Patrizia Buttol, Valentina Imbeni, Carla Martini, Giuseppe Palombarini

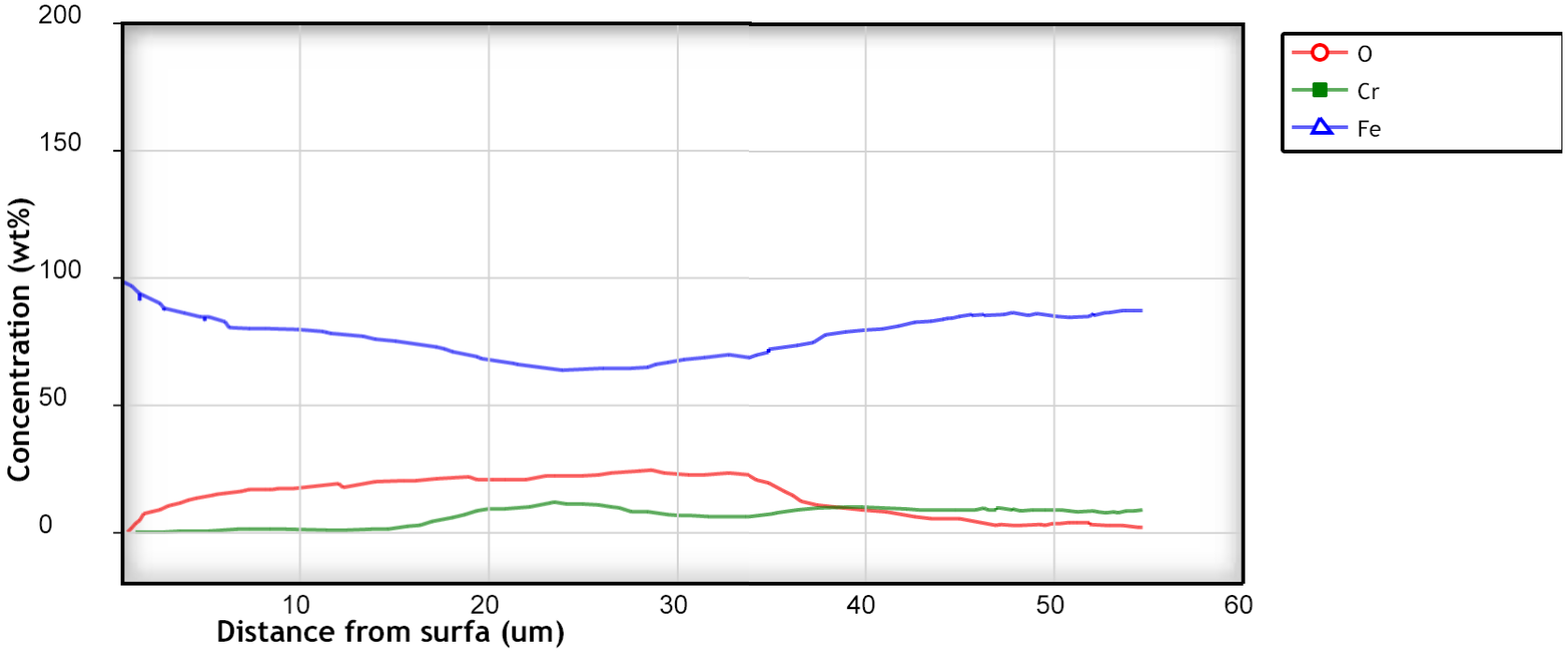

Concentration line profiles (wt%, EDS analysis with ZAF correction) on a corrosion layer grown on uncoated F82H steel after 3700 h in molten lead at 793 K

Reference:

Author: *Gianluca Benamati, Patrizia Buttol, Valentina Imbeni, Carla Martini, Giuseppe Palombarini*

Title: *Behavior of materials for accelerator driven systems in stagnant molten lead*

Source: *Journal of Nuclear Materials, 2000, Volume 279, Page 308-316*, [PDF]

View Data | Author Comments

Plot Format:

Y-Scale: ◉ linear ○ log ○ ln

X-Scale: ◉ linear ○ log ○ ln

ELSEVIER

Journal of Nuclear Materials 279 (2000) 308–316

journal of nuclear materials

www.elsevier.nl/locate/jnucmat

Behaviour of materials for accelerator driven systems in stagnant molten lead

Gianluca Benamati [a,*], Patrizia Buttol [b], Valentina Imbeni [c], Carla Martini [c], Giuseppe Palombarini [c]

[a] *Energy Department, Fusion Division, ENEA RC Brasimone, 40032 Camugnano (Bologna), Italy*

[b] *Energy Department, Sustainable Energy Systems Division, ENEA RC "E.Clementel", via Martiri di Montesole, 4-40129 Bologna, Italy*

[c] *Institute of Metallurgy, University of Bologna, viale Risorgimento, 4-40136 Bologna, Italy*

Received 13 September 1999; accepted 6 December 1999

Abstract

The behaviour of a modified F82H martensitic steel (both uncoated and aluminised) and tungsten was evaluated by immersion tests in stagnant, oxygen-saturated liquid lead at 793 K under an argon atmosphere, for exposure times up to 3700 h. The F82H steel is a candidate structural material for Accelerator Driven Systems (ADS), while tungsten is potentially suitable for a beam window working immersed in liquid lead. Layers of Me_3O_4 consisting of an inner sublayer with Me = Fe and Cr and an outer chromium-free sublayer of Fe_3O_4, formed on the surface of the uncoated steel while the aluminised steel showed no significant alteration. On tungsten, a compact and adherent layer of WO_3 formed and reacted with liquid lead leading to the formation of friable Pb–W–O ternary compounds. A two-step mechanism is proposed for interactions of metals and alloys exposed to oxygen-saturated molten lead: the first step is the solid phase oxidation of the base metal; the second is the interaction between liquid lead and the oxide layer formed on the metal surface.

1. Introduction

Accelerator Driven Systems (ADS) are an attractive option for assisting spent nuclear fuel disposal and have been widely studied within the international community. A sub-critical reactor, coupled with an accelerator that provides high energy protons for the production of neutrons from a spallation target, offers the possibility of eliminating the large quantities of plutonium, higher actinides and environmental hazardous fission products coming from commercial power plants, and also gives the opportunity of developing new and safer reactor technologies [1]. A basic R&D project, aiming to develop technologies required to design an ADS for nuclear waste transmutation was set up in Italy [2] with close reference to Rubbia's Energy Amplifier proposal. The Energy Amplifier (EA) was designed for both energy amplification and incineration of waste [3]. The nuclear burner would use either liquid lead (LL) or lead/bismuth (LLB) technology developed in the former USSR for nuclear submarine propulsion. LL and LLB would act as both nuclear coolants and spallation neutron sources. Liquid lead was chosen because of its high atomic number, good neutron yield and low vapour pressure. As compared to LL, LLB has a considerably lower melting point (398 vs 600 K), but can be more corrosive [4,5]. The corrosion rates in LL-based environments of steels, widely used as structural materials, are significantly higher than those measured in liquid alkali metals, mainly because of the high solubility of some alloying elements in lead and lead alloys [6–8]. In the present work, some preliminary compatibility tests on potential materials for ADS in stagnant LL were made in order to study the behaviour of a modified F82H martensitic steel and of pure tungsten, and also to check the effectiveness of aluminised coatings as a

* Corresponding author. Tel.: +39-0534 801 181; fax: +39-0534 801 225.

E-mail address: gianluca@netbra.brasimone.enea.it (G. Benamati).

0022-3115/00/$ - see front matter
PII: S0022-3115(99)00283-4

Table 1
Composition of the F82H steel (wt%)

C	Cr	Ni	Mo	V	Nb	Si	Mn	S
0.09	7.8	0.04	<0.01	0.16	<0.01	0.13	0.18	0.003
P	B	N	Ta	Al	Cu	W	Ti	
0.004	<0.001	0.006	0.02	<0.01	<0.007	2	<0.02	

corrosion barrier. Corrosion tests in stationary liquid metals are important as they give information on the corrosion mode of alloys, although further tests in circulating melts are essential to evaluate the corrosion behaviour of the material when erosion and mass transport are involved. The mod.F82H martensitic steel has been developed for fusion applications as a reduced activation material [9,10], while coatings constituted by Fe–Al intermetallic compounds are known to have a satisfactory thermal stability and resistance to both oxidation and corrosion at the temperatures of interest [11]. Tungsten, in turn, has been reported to have a very low solubility in molten lead [12] and to be potentially suitable for a beam window working immersed in a liquid lead spallation target [1].

2. Experimental

2.1. Materials

The composition of the F82H steel and 99.95% pure tungsten are reported in Tables 1 and 2, respectively. Specimen dimensions were $19 \times 13 \times 3$ mm^3. Steel samples were aluminised in the laboratories of IMF III–FZK, Karlsruhe, by a two-step process: hot dipping in molten aluminium at 973 K for 30 s, followed by a thermal treatment at 1313 K for 30 min and 1023 K for 1 h. The resulting coating was constituted by layers of Fe–Al intermetallic compounds, as reported in Ref. [13].

2.2. Testing procedure

The materials behaviour in molten lead was investigated by immersion tests in stagnant liquid metal at constant temperature (793 ± 5) K using alumina crucibles, in a glove-box under a high purity argon atmosphere. Two specimens of the same material were placed in each crucible in contact with molten lead over different periods of immersion time. The main impurities in the argon were O_2 (3 vppm), H_2O vapour (5 vppm) and N_2 (5 vppm). About 3 kg of solid lead was melted into each cylindrical crucible of alumina (diameter 58.5 mm, height 104 mm). The temperature was measured by chromel–alumel thermocouples placed into the liquid lead. The immersion times were 2000 and 3700 h for the aluminised and uncoated steel specimens, and 1700 and 2000 h for the tungsten ones.

Table 2
Composition of tungsten samples (wppm; purity 99.95%, supplier Goodfellow)

Ca	Cu	Fe	Mg	Mo	Ni	Pb
<20	<20	20	<10	150	<20	<50
Si	Sn	Ti	C	H	N	O
<50	<30	<20	30	6	10	30

The molten metal was saturated by oxygen, as proved by the presence of lead oxide (PbO) floating on the free surface. Measurements of total oxygen content in the lead by extraction from the melt as CO_2 and determination by an IR sensor, carried out after the tests, confirmed that lead was in all cases saturated by oxygen throughout the test. In fact, the total oxygen contents measured after the tests were in the range from 30 to 40 wppm, i.e., higher than the values reported in the literature for the solubility limit of oxygen dissolved in liquid lead at the testing temperature [14–17].

The specimens were weighed before and after the immersion tests with a precision of 10^{-2} mg, in order to detect any mass change due to corrosion or formation of reaction products. The final weight was measured after etching the samples in a 50% by volume solution of hydrogen peroxide in acetic acid to clean the specimens by residual lead and lead oxide.

The effects of immersion were studied by optical microscopy (OM), scanning electron microscopy (SEM), electron probe microanalysis (EPMA) and X-ray diffraction analysis (XRD) on the specimen surface and after a progressive removal of reaction products in order to obtain information on their distribution. The thickness of removed layers was measured by a micrometer. The XRD patterns were recorded using a computer-controlled goniometer (2θ step 0.02°, counting time 1 s) and Co-Kα radiation for the steel specimens, Cu-Kα radiation for the tungsten specimens. The EPMA measurements were carried out by the energy dispersive spectroscopy (EDS) on cross-sections of specimens prepared with the usual metallographic techniques. Observations and microanalyses were also carried out on reaction products fragments taken from surface layers.

3. Results

3.1. F82H steel

The interaction with the oxygen-saturated, molten lead led to the formation of continuous layers of reaction products on the uncoated steel surfaces. Consequently, the weight of these specimens increased during the test (Table 3).

The average thickness of the layers was $\simeq 20$ μm after 2000 h of exposure at 793 K (Fig. 1), and $\simeq 40$ μm after 3700 h of exposure at the same temperature. In contrast, no significant weight change or alteration was observed on the aluminised samples tested under the same experimental conditions and chemically cleaned.

For both exposure times, the products formed on the uncoated steel consisted of two morphologically different sublayers: an outer sublayer (labelled D in Fig. 1) which, as shown by the fractographic image reported in Fig. 2, grew with a columnar morphology; and an inner sublayer (labelled C in Figs. 1 and 2).

Table 3
Weight variations measured on tested and chemically cleaned samples

Material	Exposure time (h)	Weight variation (g)
Mod. F82H	2000	$+0.0741 \pm 0.012$
	3700	$+0.1652 \pm 0.020$
Tungsten	1700	$+0.0814 \pm 0.040$
	2000	$+0.0927 \pm 0.040$
Mod. F82H aluminised	2000	<0.0002
	3700	<0.0002

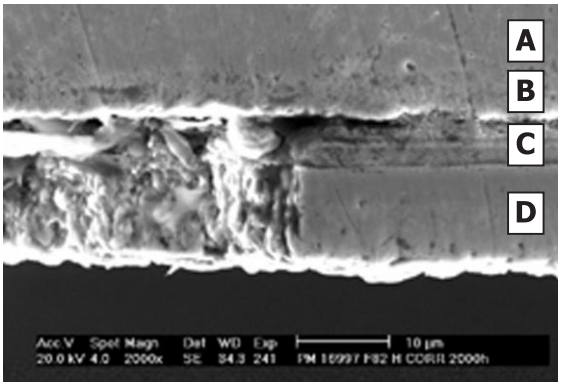

Fig. 1. Cross section of a corrosion layer grown on uncoated F82H exposed to molten lead at 793 K for 2000 h. The left side of the layer shows a fracture section (A: steel; B: Cr-depleted steel; C: Me_3O_4 with Me = Fe, Cr; D: Fe_3O_4 embedding small particles of lead).

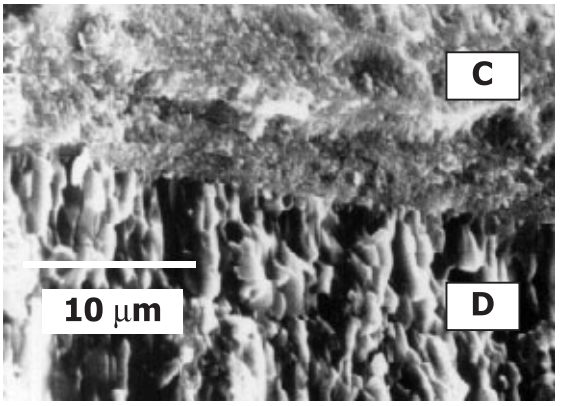

Fig. 2. Details of a detached fragment from a corrosion layer grown on uncoated F82H steel exposed to molten lead at 793 K for 3700 h (C: Me_3O_4 with Me = Fe, Cr; D: Fe_3O_4 + Pb).

Fig. 3 shows concentration profiles recorded for the layer grown in 2000 h on the uncoated steel. A depletion of chromium occurred in the region under the steel/reaction products interface. On the other hand, chromium is present in the inner sublayer of the reaction products (C in Fig. 1) and its concentration decreases on going towards the surface until it becomes negligible within the outer sublayer (D in Fig. 1). After 3700 h the chromium concentration reaches a maximum at $\simeq 30$ μm from the surface, where the iron content is minimum. Lead was detected by elemental analyses in the outer sublayers of all the product layers.

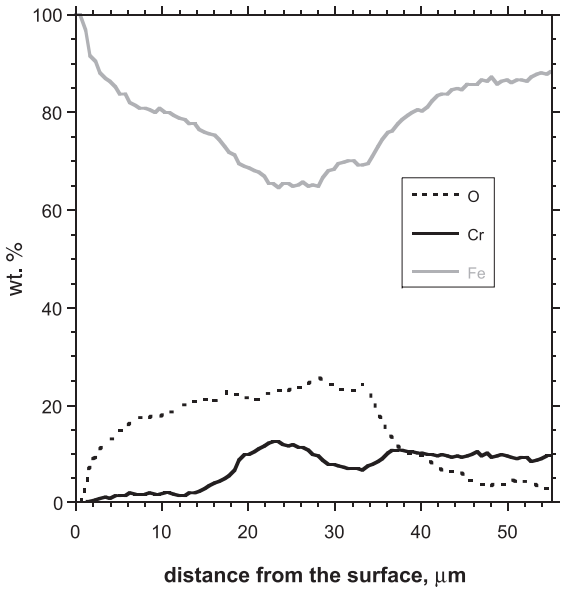

Fig. 3. Concentration line profiles (wt%, EDS analysis with ZAF correction) on a corrosion layer grown on uncoated F82H steel after 3700 h in molten lead at 793 K.

Fig. 4 shows XRD patterns recorded at different depths from the surface of a steel sample tested for 3700 h. The XRD analysis indicates that the reaction products mainly consist of Me_3O_4 (with Me = Fe and Cr, whose distribution in the two sublayers is shown by elemental analyses) and, to a less extent, of metallic lead. No Fe–Pb–O ternary compound, whose formation might be expected according to the phase diagram, was identified in the XRD patterns. The contribution of lead to the patterns decreased on going closer to the steel substrate, in agreement with the results of the elemental analyses. This suggests that, during the growth of the Me_3O_4 layer, very small particles of metallic lead were embedded in the outer columnar part of the oxide layer (sublayer D in Figs. 1 and 2).

No reaction products were detected in the XRD patterns recorded for the aluminised samples (Fig. 5). Only the formation of a protective layer of Al_2O_3, too thin to contribute to XRD patterns, could be hypothesised for this coating.

The above results show that the aluminised coating, whose characteristics are reported in Ref. [13], was able to protect the steel during the exposure to liquid, oxygen-saturated lead. This result is in agreement with

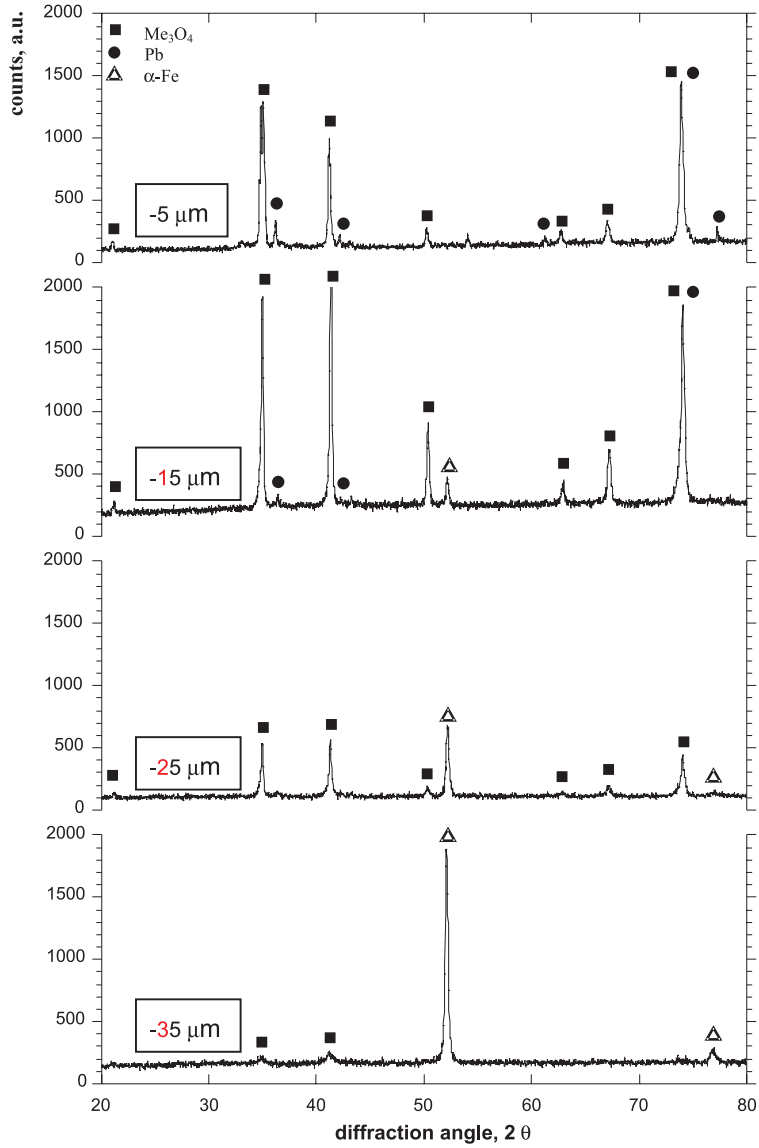

Fig. 4. XRD patterns for uncoated F82H steel after 3700 h in molten lead at 793 K, measured at decreasing distance from the external surface (Co-Kα).

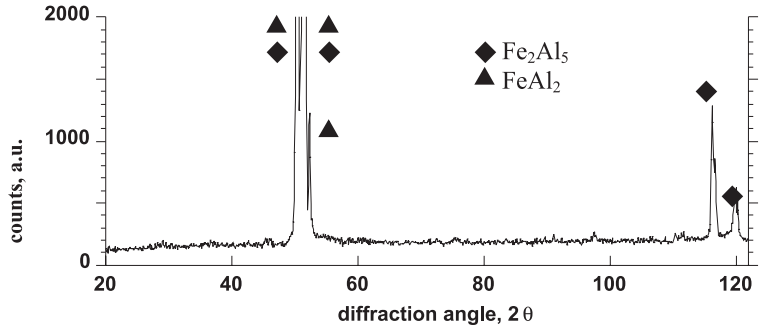

Fig. 5. XRD pattern for aluminised F82H steel after 2000 h in molten lead at 793 K (Co-Kα).

previous studies on the behaviour of aluminised steel in contact with liquid Pb–17Li eutectic alloy [18]. The behaviour of aluminised steel is to be verified under dynamic conditions.

On the contrary, the uncoated steel underwent a considerable oxidation involving both iron and chromium (the Cr content in the steel is 7.8 wt%, Table 1). By comparing the thermodynamic driving forces for the oxidation of lead, iron, chromium and aluminium, evaluated on the basis of the Gibbs energies of formation of their oxides (Fig. 6), reactions between the dissolved oxygen and the uncoated steel to give Fe_3O_4, or Cr_2O_3, or Al_2O_3, are favoured as compared to the reaction of oxygen with liquid Pb to give PbO. At 793 K, in particular, the following ΔG^0 values (in kJ/mol O_2) were calculated using data taken from [19]: −283 for PbO, −410 for Fe_2O_3, −427 for Fe_3O_4, −615 for Cr_2O_3 and −954 for Al_2O_3. Therefore, under the testing conditions the oxygen dissolved in liquid lead formed oxides of alloying elements of the uncoated steel, and was re-

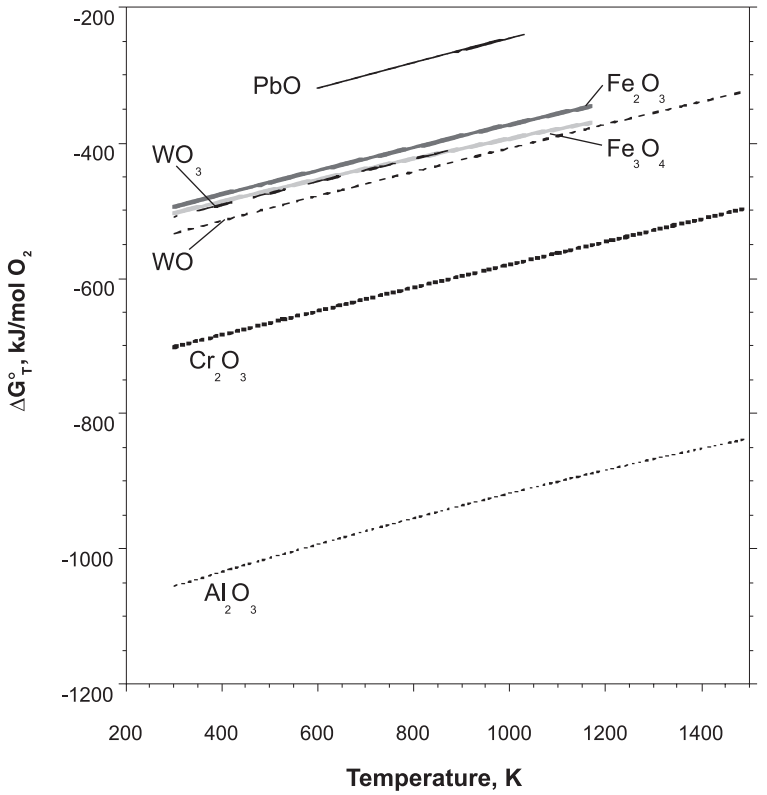

Fig. 6. Gibbs energy of formation of Fe, Cr, W, Al and Pb oxides as a function of temperature [19].

placed by oxygen liberated by the excess of lead oxide according to the reaction

$$\langle PbO\rangle \Longleftrightarrow \{Pb\} + [O]_{\{Pb\}}, \quad (1)$$

where $\langle\ \rangle$ means solid, $\{\ \}$ liquid and $[\ ]$ solution (the suffix indicating the medium).

In regard to the Cr-containing sublayer of Me_3O_4, the possible formation of the spinel $FeO\cdot Cr_2O_3$ (an Me_3O_4 oxide with Cr^{3+}as the only trivalent ion) was taken into account. As the diffraction peaks of this compound are very close to those of Fe_3O_4, the presence of this spinel was verified by EDS chemical analyses, but a concentration of Cr close to that corresponding to $FeO\cdot Cr_2O_3$ (28.57 at.%) was not observed in any of the Cr profiles, like that shown in Fig. 3. Moreover, the concentration of Cr progressively decreases on going from the interface between the steel and the oxide layer to the interface between the two Me_3O_4 sublayers. Therefore, a mechanism involving the formation of a spinel-type $(Fe, Cr)_3O_4$ solid solution containing both Fe^{3+} and Cr^{3+} ions seems to be preferred.

The formation on the uncoated steel of two distinct sublayers of Me_3O_4, only the inner one containing chromium in addition to iron, can be explained considering the limited content of chromium in the steel. The increasing of the oxide layer thickness along with the exposure time shows that the layer itself is not protective against oxidation in oxygen-saturated liquid lead containing an additional source of oxygen in the form of PbO. On the other hand, the columnar morphology of the outer, Cr-free sublayer of Fe_3O_4 might have favoured the embedding of very small particles of metallic lead.

3.2. Tungsten

The interaction with the molten, oxygen-saturated lead led to the formation of continuous layers of reaction products on the tungsten surface. Consequently, the weight of these specimens, measured after the chemical removal of the residual amounts of lead, increased during the test (Table 3), similarly to that observed for the uncoated steel tested under the same conditions. In the case of tungsten, the outer part of the product layers was friable.

The metallographic observations showed that surface layers of reaction products $\simeq$ 25 μm and $\simeq$ 30 μm thick formed in 1700 and 2000 h of exposure to liquid lead, respectively. Fig. 7 shows a cross-section of a layer grown in 2000 h. Two different sublayers (labelled F and G in Fig. 7) were generally observed in the product layers. The outer sublayer (G in Fig. 7) was friable, its compactness decreasing on going towards the external surface. This caused loss of fragments during the metallographic preparation, reducing the precision of

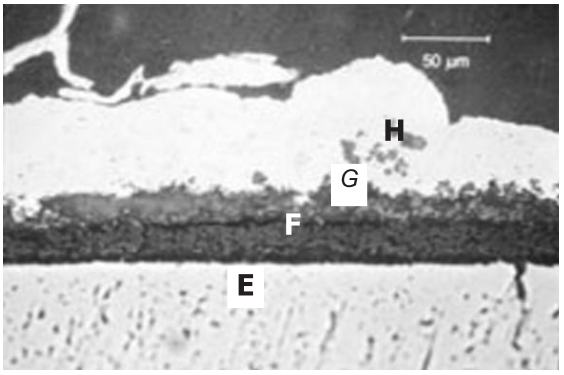

Fig. 7. Cross section of a tungsten sample exposed to molten lead for 2000 h at 793 K (E: tungsten; F: WO_3; G: $PbWO_4 + Pb_2WO_5$; H: Cu deposited for metallographic purpose).

thickness measurements. Furthermore, the outer sublayer was heterogeneous, its colour gradually turning from grey (at the interface with the inner sublayer) to white-yellow. The inner sublayer (F in Fig. 7) was very compact and adherent to the metal substrate, homogeneous and black. Its thickness ranged from $\simeq$ 10 to $\simeq$ 15 μm after 1700 h of exposure, and from $\simeq$ 15 to $\simeq$ 20 μm after 2000 h. As shown by EDS analyses (Fig. 8), the inner sublayer (F in Fig. 7) contained tungsten and oxygen, while the outer sublayer (G in Fig. 7) contained tungsten, oxygen and lead.

The XRD patterns, also recorded after careful removal of reaction products from the surface, showed that the following reaction products were formed on tungsten: WO_3, grown with a (0 0 1) preferred orientation, and two W–Pb–O ternary compounds, $PbWO_4$ and Pb_2WO_5 (Figs. 9 and 10). The analysis at different depths allowed to deduce that the inner, compact and adherent sublayer of reaction products on tungsten (F in

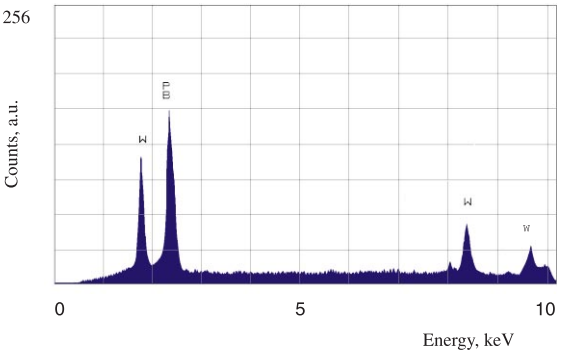

Fig. 8. EDS analysis on particles removed from the outer part of the corrosion products grown on tungsten exposed to molten lead for 2000 h at 793 K.

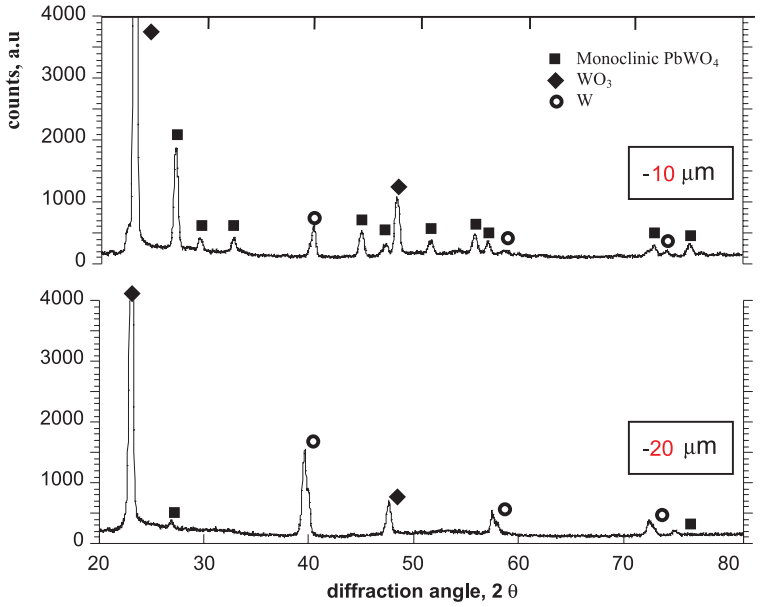

Fig. 9. XRD patterns for tungsten in molten lead at 793 K after 1700 h (Cu-Kα), measured at decreasing distances from the surface in order to avoid contributions from Pb–W–O ternary compounds.

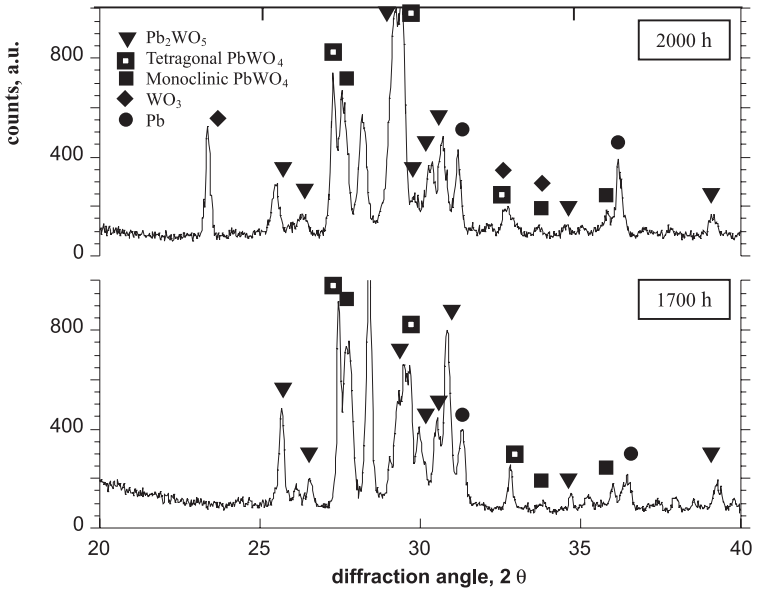

Fig. 10. XRD patterns for tungsten exposed for different times to molten lead at 793 K (Cu-Kα). The 2θ range was limited because of the high number of peaks. Markers indicate attributed peaks.

Fig. 7) was constituted by WO_3, while the outer sublayer (G in Fig. 7) consisted of the above mentioned W–Pb–O ternary compounds.

It is to be noted that, according to the W–O phase diagram [20], the formation of the WO_2 oxide would be expected at the interface with the base metal (Fig. 6). In particular, at 793 K the ΔG^0 values of formation for WO_2 and WO_3, calculated (in kJ/mol O_2) using data taken from [19], are −443 for WO_2 and −424 for WO_3, to be compared with −283 kJ/mol O_2 previously calcu-

lated for the formation of PbO. However, at temperatures below about 873 K and in conditions far from equilibrium, WO_3 is reported to be the oxide formed in contact with tungsten [21,22]. This suggests that also the metal-oxide system under examination might be out of equilibrium notwithstanding the long time of exposure (2000 h), e.g., for the resistance opposed by the oxidised layer to the diffusion of oxygen from lead to tungsten.

Therefore, also in the case of tungsten in contact with LL the dissolved oxygen was consumed to form oxidised products, and was replaced by the oxygen liberated by the excess of lead oxide, which was an additional source of oxygen for the reaction. Notwithstanding its compactness and adherence to the base metal, the layer of WO_3 was unable to protect the base metal against further oxidation. In fact, liquid Pb reacted with WO_3 leading to the formation of Pb–W–O ternary compounds. Because of their poor compactness these ternary products are easily detached from the substrate and the oxidation of tungsten proceeds. The formation of Pb–W–O ternary compounds should be verified in flowing systems with a controlled content of oxygen.

4. Conclusions

The study of the behaviour of a modified F82 steel (both uncoated and aluminised) and tungsten behaviour by immersion tests in stagnant liquid, oxygen-saturated lead led to the following conclusions.

(1) The presence of oxygen in molten lead modifies the basic mechanism of metal corrosion (i.e. direct dissolution of one or more alloying elements into the liquid metal) because of the formation of oxidation products. The uncoated steel and tungsten oxidised considerably in 2000 h of exposure, while the aluminised steel underwent no significant alteration after the same time. Therefore, protection of structural steels from elemental dissolution and corrosion in liquid lead by coatings constituted by Fe–Al intermetallic compounds is possible.

(2) A two-step mechanism is proposed for the oxidation of uncoated steel and tungsten: the first step is the oxidation of the base metal exposed to liquid lead, which leads to the formation of a layer of Me_3O_4 on the steel, and a layer of WO_3 on tungsten. The layer of Me_3O_4 was constituted by two sublayers, the inner of $(Fe,Cr)_3O_4$ (i.e. Me_3O_4 with Me = Fe and Cr), the outer of Fe_3O_4. The second step is the interaction between liquid lead and these oxide layers. Under the adopted conditions of exposure (temperature, time and liquid metal saturation), this step led to the formation of ternary compounds in the case of tungsten samples.

(3) Special care has to be taken in selecting metals to be used in contact with oxygen-containing molten lead. The solubility of alloying elements in molten lead is not the only key-parameter. The adherence, compactness and protectiveness of the oxide layers should be also taken into account, together with their reactivity with molten metal. Further corrosion experiments in dynamic conditions have to be performed in order to fully evaluate the materials performance under in-service conditions.

Acknowledgements

The authors wish to thank Dr H. Glasbrenner for preparing and providing specimens of aluminised steel. The research was financially supported by ENEA-INFN and MURST (TRASCO project), Rome, Italy.

References

[1] J.C. Brown, F. Venneri, N. Li, M.A. Williamson, Accelerator-driven transmutation of waste, White Paper, Los Alamos National Laboratory, 2 February 1998.
[2] G. Gherardi, S. Monti, in: Proceedings of the OECD-NEA-NSC Workshop on Utilisation and Reliability of High Power Proton Accelerators, Jaeri, Tokai-Mura, Japan, October 1998, pp. 12–15.
[3] C. Rubbia, J.A. Rubio, S. Buono, F. Carminati, N. Fìetier, J. Galvez, C. Gelès, Y. Kadi, R. Klapish, P. Mandrillion, J.P. Revol, C. Roche, Conceptual design of a fast neutron operated high power energy amplifier, European Organization for Nuclear Research, CERN Report AT/95-44 (ET), 1995.
[4] B.F. Gromov, Yu.I. Orlov, P.N. Martynov, K.D. Ivanov, V.A. Gulevsky, in: H.U. Borgstedt, G. Frees (Eds.), Liquid Metal Systems, Plenum, New York, 1995, p. 339.
[5] J.R. Weeks, Nucl. Eng. Des. 15 (1971) 363.
[6] R.C. Asher, D. Davies, S.A. Beetham, Corros. Sci. 17 (1977) 545.
[7] P.F. Tortorelli, O.K. Chopra, J. Nucl. Mater. 103&104 (1981) 621.
[8] I. Ali-Khan, in: Proceedings of the Conference on Metals in Liquid Lead: Material Behaviour and Physical Chemistry in Liquid Metal Systems, Karlsruhe, D, March 1981, p. 243.
[9] T. Noda, F. Abe, H. Araki, M. Okada, J. Nucl. Mater. 155–167 (1988) 581.
[10] E.E. Bloom, D.S. Gelles, R.L. Klueh, in: Proceedings of the IEA Workshop on Low Activation Materials, IEA, Paris (Culham, UK, April 1991).
[11] H.U. Borgstedt, H. Glasbrenner, Fusion Eng. Des. 27 (1995) 659.
[12] C. Guminski, Z. Metallkd. 81 (1990) 105.
[13] H. Glasbrenner, J. Konys, K. Stein-Fechner, O. Wedemeyer, J. Nucl. Mater. 258–263 (1998) 1173.
[14] C.B. Alcock, T.N. Belford, Trans. Farad. Soc. 60 (1964) 822.
[15] A. Taskinen, Scand. J. Metall. 8 (1982) 185.
[16] Yu.I. Orlov, B.F. Gromov, V.A. Gylevskiy, in: Seminar on the Concept of Lead Cooled Fast Reactors, CEA, Cadar-

ache, F, 22–23 September 1997 (quoted in ENEA Rept. VT-SBA-00001, December 1997, p. 134).
[17] H.A. Wriedt, Bull. Alloy Phase Diagrams 9 (1988) 106 (reported in: T.B.Massalski (Ed.), Binary Alloys Phase Diagrams, second ed., ASM International, 1990, p. 2901).
[18] G. Benamati, N. Elmi, M. Agostini, J. Nucl. Mater. 212–215 (1994) 1557.
[19] O. Kubaschewski, C.B. Alcock, P.J. Spencer, Materials Thermochemistry, 6th Ed., Pergamon, Oxford, 1993, p. 257.
[20] A.S.M. Handbook, Alloy Phase Diagrams 3 (1992) 235.
[21] J. Bénard, Oxidation des Métaux, vol. II, Gauthier-Villars, Paris, 1964, p. 251.
[22] A. Warren, A. Nylund, J. Olefjord, Int. J. Refract. Met. Hard Mater. 14 (1996) 345.